THE ASTROPHYSICAL JOURNAL, 560:566–579, 2001 October 20

THE K-BAND GALAXY LUMINOSITY FUNCTION[1,2]

C. S. KOCHANEK, M. A. PAHRE,[3] E. E. FALCO, J. P. HUCHRA, AND J. MADER
Harvard-Smithsonian Center for Astrophysics, 60 Garden Street, Cambridge, MA 02138; ckochanek@cfa.harvard.edu, mpahre@cfa.harvard.edu, efalco@cfa.harvard.edu, jhuchra@cfa.harvard.edu, jmader@cfa.harvard.edu

T. H. JARRETT, T. CHESTER, AND R. CUTRI
Infrared Processing and Analysis Center, MS 100-22, California Institute of Technology, Pasadena, CA 91125; jarrett@ipac.caltech.edu, tchester@ipac.caltech.edu, roc@ipac.caltech.edu

AND

S. E. SCHNEIDER
Department of Astronomy, University of Massachusetts, Amherst, MA 01003; schneider@messier.astro.umass.edu
Received 2000 November 22; accepted 2001 June 13

ABSTRACT

We measured the K-band luminosity function using a complete sample of 4192 morphologically typed 2MASS galaxies with $\mu_{K_s} = 20$ mag arcsec^{-2} isophotal magnitudes $7 < K_{20} < 11.25$ mag spread over 2.12 sr. Early-type ($T \leq -0.5$) and late-type ($T > -0.5$) galaxies have similarly shaped luminosity functions, $\alpha_e = -0.92 \pm 0.10$ and $\alpha_l = -0.87 \pm 0.09$. The early-type galaxies are brighter, $M_{K*e} = -23.53 \pm 0.06$ mag compared to $M_{K*l} = -22.98 \pm 0.06$ mag, but less numerous, $n_{*e} = (0.45 \pm 0.06) \times 10^{-2}$ h^3 Mpc^{-3} compared to $n_{*l} = (1.01 \pm 0.13) \times 10^{-2}$ h^3 Mpc^{-3} for $H_0 = 100$ h km s^{-1} Mpc^{-1}, such that the late-type galaxies slightly dominate the K-band luminosity density, $j_{\rm late}/j_{\rm early} = 1.17 \pm 0.12$. Including a factor of 1.20 ± 0.04 correction for the conversion of the isophotal survey magnitudes to total magnitudes, the local K-band luminosity density is $j = (7.14 \pm 0.75) \times 10^8$ h $L_\odot$ Mpc^{-3}, which implies a stellar mass density relative to critical of $\Omega_* h = (1.9 \pm 0.2) \times 10^{-3}$ for a Kennicutt initial mass function (IMF) and $\Omega_* h = (3.4 \pm 0.4) \times 10^{-3}$ for a Salpeter IMF. Our morphological classifications are internally consistent, are consistent with previous classifications, and lead to luminosity functions unaffected by the estimated uncertainties in the classifications. These luminosity functions accurately predict the K-band number counts and redshift distributions for $K \lesssim 18$ mag, beyond which the results depend on galaxy evolution and merger histories.

Subject headings: cosmology: observations — galaxies: distances and redshifts — galaxies: luminosity function, mass function — surveys

On-line material: machine-readable table

1. INTRODUCTION

The luminosity function (LF) of galaxies and its parameters, dependence on galaxy type, and evolution are fundamental to observational cosmology and the theory of galaxy formation. Most existing estimates of the LF are based on redshift surveys of galaxies selected from blue photographic plates (CfA/CfA2, Davis & Huchra 1982; de Lapparent, Geller, & Huchra 1989; Geller & Huchra 1989; Marzke et al. 1994a; Marzke, Huchra, & Geller 1994b; SSRS2, da Costa et al. 1994, 1998; Marzke et al. 1998; APM, Loveday et al. 1992; ESO Slice, Vettolani et al. 1997; Zucca et al. 1997; Durham/UKST, Ratcliffe et al. 1998; Nearby Optical Galaxy Survey, Marinoni et al. 1999; 2dFGRS, Folkes et al. 1999; Slonim et al. 2001; Cross et al. 2001). The LF derivations are usually based on samples of $\sim$5000 galaxies. Blue surveys emphasize galaxies with active star formation and are sensitive to both Galactic and internal extinction, and those based on photographic plates usually have large photometric uncertainties (0.2–0.4 mag). Deep, blue-selected surveys must also include strong, type-dependent k-corrections. The only ongoing blue survey is the 2dFGRS of 250,000 galaxies.

Most recent surveys have shifted to selecting galaxies in the red, which somewhat reduces the effects of extinction and leads to samples less influenced by recent star formation. The Century Survey (Geller et al. 1997) used objects selected from red photographic plates with the photometry recalibrated by R_C-band drift scans, while the Las Campanas Redshift Survey (LCRS; Shectman et al. 1996; Lin et al. 1996; Bromley et al. 1998) selected the galaxies from Gunn r-band drift scans calibrated to approximate Kron-Cousins R_C. The Sloan Digital Sky Survey (SDSS) will obtain a surface brightness limited sample to $r' = 17.7$ mag with approximately 10^6 galaxies (see York et al. 2000) with an initial estimate of the LF by Blanton et al. (2001).

Infrared galaxy surveys have smaller systematic uncertainties than optical galaxy surveys. They are almost immune to both Galactic and internal extinction, and the k-corrections and luminosity per unit stellar mass are nearly independent of galaxy type (e.g., Cowie et al. 1994; Gavazzi, Pierini, & Boselli 1996). The determination of infrared LFs has proceeded slowly, however, because of the difficulty of obtaining large complete samples. Mobasher, Sharples, & Ellis (1993) and Loveday (2000) obtained infrared photometry of optically selected galaxies to estimate the infrared LF. Glazebrook et al. (1994, 1995), Gardner et al. (1997), and Szokoly et al. (1998) used relatively deep IR surveys of

[1] This publication makes use of data products from the Two Micron All Sky Survey (2MASS), which is a joint project of the University of Massachusetts and the Infrared Processing and Analysis Center/California Institute of Technology, funded by the National Aeronautics and Space Administration and the National Science Foundation.

[2] This research has made use of the NASA/IPAC Extragalactic Database (NED), which is operated by the Jet Propulsion Laboratory, California Institute of Technology, under contract with the National Aeronautics and Space Administration.

[3] Hubble Fellow.

small regions, where the faintness of the targets makes it difficult to obtain redshifts of the full sample. Andreon & Pello (2000) and de Propris et al. (1998) have also estimated the infrared LF by constructing volume-limited samples of galaxies in the Coma Cluster. The resulting samples are typically 10 times smaller than published optical samples (~ 500 rather than ~ 5000 galaxies).

The 2MASS project (Skrutskie et al. 1997) is obtaining a complete infrared map of the sky, with a limiting magnitude for its galaxy catalog of $K_s \simeq 13.5$ mag. Since 2MASS overlaps the existing optical surveys, it is easy to generate large, complete redshift surveys of 2MASS-selected galaxies rapidly. In this paper we discuss a redshift survey of 2MASS galaxies overlapping the CfA2 survey and the updated Zwicky catalog (UZC; Falco et al. 1999). To our magnitude limit, $\sim 90\%$ of the galaxies already had redshifts and the remainder were obtained as part of our redshift survey. A similar strategy was adopted by Cole et al. (2001), who combined the 2MASS photometric survey with the 2dFGRS redshift survey. For the first time we can derive infrared LFs from samples of comparable size to that of the published optical LFs. In § 2 we discuss the sample selection, in § 3 we derive the LF by galaxy type, and in § 4 we estimate the local infrared luminosity density. In § 5 we compare the results to other estimates of the LF, and in § 6 we use our LFs to predict the properties of fainter infrared galaxy samples. We summarize our results in § 7.

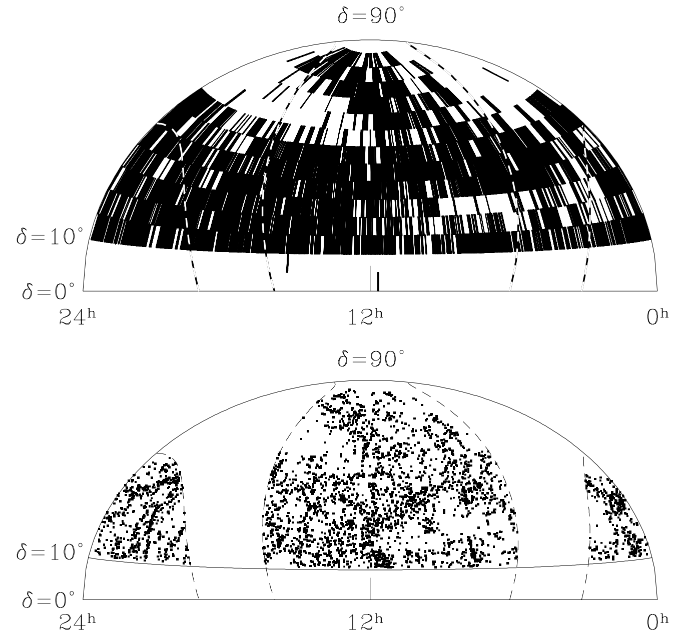

FIG. 1.—Aitoff projections of the 2MASS scan coverage (*top*) and the sample galaxies (*bottom*) in equatorial coordinates. The dashed lines show the $|b| \geq 20°$ Galactic latitude limits, and the solid line shows the lower declination limit at $\delta \geq 10°$.

2. SAMPLE SELECTION AND DATA

We selected 4353 targets from the 2MASS Second Incremental Release Catalog of Extended Sources using the default K_s-band survey magnitude, K_{20}, which is the magnitude inside the circular isophote corresponding to a surface brightness of $\mu_{K_s} = 20$ mag arcsec^{-2} (see Jarrett et al. 2000a). We discuss the properties of the photometric catalog, the selection of the K_{20} magnitude for our survey, and its relationship to total magnitudes in the Appendix. An offset of $\Delta = -0.20 \pm 0.04$ mag must be added to the K_{20} isophotal magnitudes to convert to total magnitudes (see Appendix; Jarrett et al. 2000a). We selected all extended sources with $7 \leq K_{20} \leq 11.25$ mag, $\delta \geq 11°$ (J2000), and $|b| \geq 20°$, modulated by the actual sky coverage of the release (see Fig. 1). Although there is no exact correspondence to optical redshift surveys because of the wide range of optical-to-infrared galaxy colors, our magnitude limit roughly corresponds to $B \lesssim 15$ mag or $R_C \lesssim 14$ mag. The effective optical limits are deeper for red early-type galaxies and shallower for blue late-type galaxies. Objects that were not galaxies (artifacts, double stars, planetary nebulae, etc.) were removed from the sample by inspection of the 2MASS data flags and images, the NED databases, and digitized POSS-II[4,5] images of the targets, leaving a sample of 4192 galaxies. We determined the survey area by integrating over the survey scans (the scans are $8'.5 \times 6°$). Note that the lower boundary of the scanned region actually lies between $11°.5$ and $12°$ in declination. The scanned regions inside the angular boundaries cover $\Delta\Omega = 2.12$ sr, which is $\frac{2}{3}$ of the area inside the boundaries. The uncertainties in the survey area are less than 5%, but they are difficult to estimate precisely because they depend on the detailed treatment of galaxies near the edges. A few percent of the area is also masked by bright stars.

Since the survey region overlaps the CfA2 redshift survey (Geller & Huchra 1989) and the UZC (Falco et al. 1999), almost all the galaxies in the sample had known redshifts. We based our redshift catalog on ZCAT[6] (Huchra et al. 1992) but checked the redshifts against the UZC reanalysis of the CfA/CfA2 redshift survey and reconciled or corrected any significant disagreements between the two redshift catalogs. The galaxies lacking redshifts were primarily elliptical galaxies whose Zwicky magnitudes were fainter than the UZC magnitude limit and galaxies outside the CfA survey area but inside our Galactic latitude limits. We obtained the missing redshifts using the FLWO Tillinghast 1.5 m telescope, the FAST spectrograph (Fabricant et al. 1998), and standard reduction procedures (Kurtz & Mink 1998). Figure 1 shows an Aitoff projection of the galaxy sample.

The morphological types of the galaxies are important for studies of galaxy evolution (e.g., Lilly et al. 1995) and the differences between galaxy environments (e.g., Dressler 1980). Our galaxies are relatively nearby, which allows us to classify the galaxies morphologically. Of the 4192 galaxies, only 1673 have unambiguous types in the RC3 catalog (de Vaucouleurs, de Vaucouleurs, & Corwin 1976). Each galaxy was visually classified by at least two of the authors (E. E. F., J. P. H., C. S. K., and M. A. P. did the classification)

[4] The Second Palomar Observatory Sky Survey (POSS-II) was made by the California Institute of Technology with funds from the National Science Foundation, the National Geographic Society, the Sloan Foundation, the Samuel Oschin Foundation, and the Eastman Kodak Corporation. The Oschin Schmidt Telescope is operated by the California Institute of Technology and Palomar Observatory.

[5] The Digitized Sky Surveys were produced at the Space Telescope Science Institute under US Government grant NAG W-2166. The images of these surveys are based on photographic data obtained using the Oschin Schmidt Telescope on Palomar Mountain and the UK Schmidt Telescope. The plates were processed into the present compressed digital form with the permission of these institutions.

[6] http://cfa-www.harvard.edu/~huchra/zcat.

using digitized POSS-II images (POSS-I[7] for the small fraction where POSS-II was unavailable). The galaxies were assigned to the classifiers randomly and without information on the classifications from RC3 or the other classifiers. We did not, in general, make use of the full range of fine distinctions in the T-type scale for early-type galaxies and very late type galaxies. Most classifiers used E, E/S0, and S0 for early-type galaxies (rather than cE, E, E+, S0−, S0, and S0+), and the very late type galaxy classifications (Sd, Sdm, Sm, and Im) were not applied uniformly. T types are more finely grained than we ultimately require, and our classifications will be internally consistent viewed as the sequence E, E/S0, S0, S0/a, Sa, Sab, Sb, Sbc, Sc, Scd, Sd+later. Flags were added for bars ("B"), possible bars ("X"), peculiar morphologies ("Pec"), and evidence for overlapping or interacting neighboring galaxies ("Int"). Our philosophy for interacting and peculiar galaxies was to assign our best estimate of the "intrinsic" morphology rather than classifying based on the transient structures created by the interaction. The flags were set whenever one classifier assigned it to the galaxy, and they should be regarded as indicative but not as statistically reliable as the galaxy types because they were not subject to the same level of inspection.

Once the preliminary classifications were complete, we reconsidered the galaxies with classification ranges covering more than four T types (about 10% of the galaxies). These galaxies were reclassified by all four classifiers with knowledge of all the classifications. The worst cases were dominated by interacting galaxies, galaxies with odd star formation patterns, galaxies classified as "Irr" meaning "peculiar" rather than "Im" ($T = 10$) in RC3, and the fine-grained nature of the early and very late T types. Galaxies with type ranges greater than five T types were individually discussed. A small number (28 of 1673, or 1.7%) of RC3 classifications, largely galaxies classified as "Irr" (13 of the 28), were deleted. The final classification was the average T type of all the classifications. Figure 2 compares our internal classifications and the RC3 classifications for the galaxies in both samples, as a function of the RC3 T type. The average difference between the RC3 T types and our average T types is 0.01 with a dispersion of 1.6, while the average differences between the individual classifiers and RC3 ranged from −0.28 to 0.24 with dispersions of 1.8 T types. These statistics closely resemble the results found by Naim et al. (1995a, 1995b) when comparing morphological classifications of a range of observers and a neural network, and the biases and scatter are dominated by the very early type and very late type galaxies where we had not attempted to recreate closely the RC3 classification system. We will divide our sample into early-type and late-type galaxies at $T = -0.5$, so our systematic uncertainties will be dominated by the classification errors for S0, S0/a, and Sa galaxies (see Fig. 2). The galaxy sample is presented in Table 1.

The conversion from apparent to absolute magnitude,

$$M_K = K_{20} - 5 \log \left[\frac{D_L(z)}{r_0}\right] - R_K E(B-V) - k(z) , \quad (1)$$

has terms for the distance modulus, Galactic extinction $A_K = R_K E(B-V)$, and the k-correction $k(z)$. The luminosity

[7] The National Geographic Society–Palomar Observatory Sky Atlas (POSS-I) was made by the California Institute of Technology with grants from the National Geographic Society.

TABLE 1

THE GALAXY SAMPLE

Target	cz (km s^{-1})	Reference Code	K_{20} (mag)	T Type	Bar	Pec?	Int?
2MJ000009.1+324418......	10372	2779	10.59	−4.2±1.3			
2MJ000028.8+324656......	9803	2700	10.89	−4.9±0.1			Y
2MJ000038.0+282305......	8705	2212	10.52	1.5±0.9			
2MJ000044.0+282405......	8157	2779	11.22	2.3±1.0	B		Y
2MJ000047.0+282407......	8764	2779	10.33	−4.0±1.5			Y
2MJ000058.9+285442......	6899	2212	11.09	2.0±1.0	X		
2MJ000103.6+343911......	12684	−160	11.16	2.0±1.0			
2MJ000114.1+344032......	12953	2779	11.08	3.0±1.0	BX		Y
2MJ000119.7+343132......	5032	5502	10.62	2.5±1.0			
2MJ000126.7+312600......	4948	2700	10.26	−3.5±1.5	X	Y	Y
2MJ000130.0+312630......	4767	2212	10.42	3.7±1.0		Y	Y
2MJ000138.3+232902......	4371	0620	9.27	5.1±0.1			Y
2MJ000141.9+232944......	4336	0620	9.94	4.6±0.9		Y	Y
2MJ000246.0+185311......	7882	0650	10.86	1.7±1.0	X		
2MJ000309.6+215736......	6600	2212	10.49	2.5±0.9		Y	
2MJ000329.2+272106......	7690	2700	11.06	0.1±1.5	X		
2MJ000335.0+231202......	7254	0668	10.97	4.4±1.0	X		
2MJ000358.7+204502......	2310	0658	8.57	4.6±0.9			
2MJ000433.7+281805......	8785	2700	10.61	−3.0±1.5			
2MJ000548.3+272657......	7531	0624	10.92	3.0±1.0	B		

NOTE.—The first 20 entries of the catalog. The redshift cz is the measured heliocentric velocity, and K_{20} is the isophotal apparent magnitude (see Jarrett et al. 2000a). The ZCAT format reference code for the source of the redshift measurement is given in the third column (see http://cfa-www.harvard.edu/~huchra/zcat/zsource.tex). The error bar on the T-type classification is the standard error based on the scatter in the two or more classifications for the object. In the "Bar" column we flag objects that at least one classifier flagged as having a full (B) or incipient bar (X). In the "Pec?" and "Int?" columns we flag objects that were considered to be peculiar or interacting by at least one classifier. Table 1 is published in its entirety in the electronic edition of the *Astrophysical Journal*. A portion is shown here for guidance regarding its form and content.

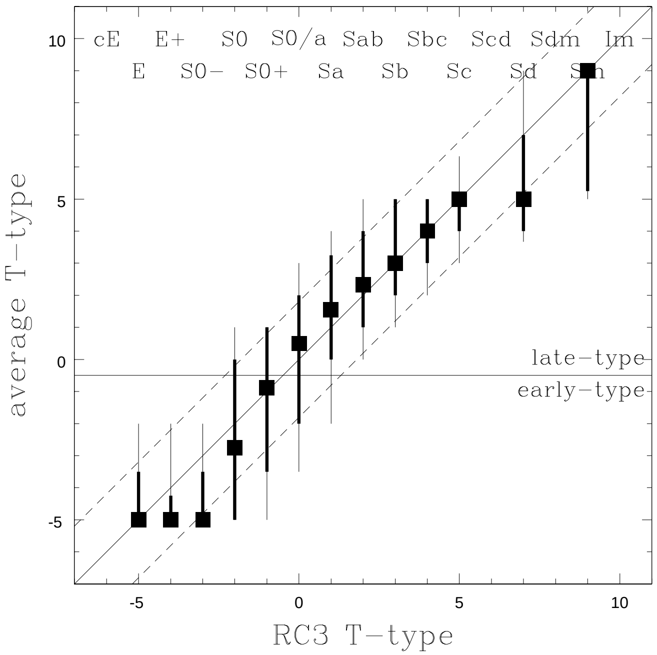

FIG. 2.—We show the median (*filled squares*), 1 σ range (*thick error bars*; 68.3% of galaxies), and 2 σ range (*thin error bars*; 95.4% of galaxies) of our classifications as a function of the RC3 T type for the 2MASS galaxies found in the RC3 catalog. The dashed lines show the typical 1.8 dispersion in T-type classifications found by Naim et al. (1995a 1995b), and the horizontal line shows where we break the sample into early-type and late-type galaxies for determining the LF. Most of the 2MASS classifiers did not use the full range of T types available for early-type galaxies (S0 and earlier) and extremely late type galaxies (Sd and later), leading to the differences at the edges of the T-type scale. These differences have no effect on our division of the sample into early- and late-type galaxies.

distance is $D_L(z) = 6000\ h^{-1}[1 + z - (1 + z)^{1/2}]$ Mpc for Hubble constant $H_0 = 100\ h$ km s^{-1} Mpc^{-1} and assuming $\Omega_0 = 1$, although the particular cosmological model is unimportant given our median redshift of $cz = 7000$ km s^{-1}. The galaxy magnitudes were corrected for Galactic extinction using the extinction maps of Schlegel, Finkbeiner, & Davis (1998) and an extinction coefficient of $R_K = 0.35$, where $A_K = E(B-V)R_K$ (Cardelli, Clayton, & Mathis 1989). The Galactic extinction was less than $E(B-V) = 0.03$ mag (0.14 mag) for 50% (95%) of the sample, and the maximum extinction was $E(B-V) = 0.64$ mag. Thus, although we include the extinction corrections, they are of little importance. The K_s-band k-correction of $k(z) = -6.0 \log(1 + z)$ is negative, independent of galaxy type, and valid for $z \lesssim 0.25$ (based on the Worthey 1994 models). Because of their negative k-correction, infrared isophotal magnitudes largely avoid the redshift-dependent biases to which Blanton et al. (2001) attribute many of the problems in the older optical surveys. Unlike most previous estimates of the local LF, our intrinsic photometric errors make a negligible contribution to the uncertainties in the LF calculation. The median error in K_{20} for our sample is 0.03 mag, and 90% of the galaxies have errors less than 0.04 mag. These estimates are verified through repeated scans of several areas on well-separated nights (T. Jarrett et al. 2000, in preparation). Our isophotal magnitudes are offset by $\Delta = -0.20 \pm 0.04$ mag from the total magnitude, and at this precision we found no dependence on the galaxy type.

Given the low redshift of our sample, we need to include corrections for peculiar velocities in the redshift estimates. We corrected the heliocentric radial velocities using the local flow model of Tonry et al. (2000). While the Tonry et al. (2000) model is computed using a different cosmology and Hubble constant, we use it only as a means of estimating the peculiar velocity corresponding to a given heliocentric velocity. For our standard analysis we restrict the sample to galaxies with corrected velocities exceeding $cz > 2000$ km s^{-1}. This velocity limit eliminates the Virgo Cluster from the sample at the price of a significant reduction in the luminosity range of the galaxies in the sample. We also analyzed the sample down to $cz > 1000$ km s^{-1}, which includes the Virgo Cluster and extends the LF determination to significantly fainter magnitudes at the price of including galaxies whose luminosities include a significant dependence on the local flow corrections.

3. THE LUMINOSITY FUNCTION

We used the standard parametric (Sandage, Tammann, & Yahil 1979) and nonparametric stepwise maximum likelihood (SWML; Efstathiou, Ellis, & Peterson 1988) methods for determining the shape of the LF, as well as the Davis & Huchra (1982) minimum variance estimator for determining the absolute number density. These methods are almost universally used for galaxy LF determinations (see Lin et al. 1996 and references therein). The completeness of the sample and the negligible magnitude errors considerably simplify the analysis over most recent studies. We used the Schechter (1976) parametric model,

$$\frac{dn}{dL} = \frac{n_*}{L_*}\left(\frac{L}{L_*}\right)^{\alpha} \exp\left(\frac{-L}{L_*}\right), \qquad (2)$$

for the Sandage et al. (1979) method fits. For our standard fits we estimated the LF using galaxies with flow-corrected velocities $cz > 2000$ km s^{-1}, which excludes the bulk of the Virgo Cluster and restricts us to galaxies with absolute magnitudes brighter than $M_K < -20.2$ mag. The density normalization was determined using the velocity range $2000 < cz < 14{,}000$ km s^{-1} and the absolute magnitude range $-25 < M_K < -22$ mag. We set the second moment of the correlation function, needed to estimate the effects of sample variance on the galaxy density, to $J_3 = 10^4(h^{-1}$ Mpc$)^3$ (Lin et al. 1996). We also show fits using galaxies with $cz > 1000$ km s^{-1}, which extends our absolute magnitude range to $M_K < -18.7$ mag at the price of increased sensitivity to errors in the velocity corrections. We have 3878 (4096) galaxies left in the sample with the velocity limit $cz > 2000$ km s^{-1} (1000 km s^{-1}). Our redshift and magnitude limits also remove almost all the large galaxies ($\gtrsim 2'$), which have unreliable magnitude estimates in the 2MASS Second Incremental Release. The LF estimation software was tested using synthetic catalogs drawn from a Poisson spatial distribution of galaxies selected from Schechter LFs. The SWML binned LFs are presented in Table 2, and the Schechter function model LFs are presented in Table 3.

Figure 3 shows LFs for the full sample, the early-type galaxies, and the late-type galaxies using the two different estimation methods. Early-type galaxies were defined to be all galaxies with $T \leq -0.5$ so that S0/a galaxies are counted as late-type galaxies and S0+ galaxies are counted as early-type galaxies. Because the distributions of the T-type classifications are somewhat quantized, the exact location of the boundary between $-1 < T < 0$ has little effect on the results. The LFs found for the $cz > 2000$ and

TABLE 2

2MASS Nonparametric Luminosity Functions

M_K (mag)	All N	All log n	All σ	Early-Type N	Early-Type log n	Early-Type σ	Late-Type N	Late-Type log n	Late-Type σ
−26.00......	1	−6.34	0.66	4	−5.93	0.36	...	...	...
−25.75......	9	−5.36	0.32						
−25.50......	16	−4.98	0.27	37	−4.84	0.17	3	−5.81	0.45
−25.25......	41	−4.42	0.23						
−25.00......	94	−3.92	0.21	160	−3.97	0.13	33	−4.54	0.15
−24.75......	169	−3.56	0.20						
−24.50......	308	−3.19	0.20	389	−3.38	0.12	173	−3.71	0.10
−24.25......	356	−3.01	0.20						
−24.00......	494	−2.74	0.20	457	−3.06	0.12	471	−3.09	0.09
−23.75......	494	−2.59	0.20						
−23.50......	437	−2.47	0.20	359	−2.83	0.12	529	−2.76	0.08
−23.25......	401	−2.32	0.20						
−23.00......	327	−2.25	0.20	210	−2.71	0.12	428	−2.51	0.08
−22.75......	206	−2.25	0.20						
−22.50......	191	−2.12	0.20	94	−2.65	0.12	261	−2.39	0.08
−22.25......	127	−2.11	0.20						
−22.00......	65	−2.15	0.21	43	−2.52	0.13	106	−2.39	0.09
−21.75......	43	−2.09	0.21						
−21.50......	33	−2.04	0.22	16	−2.49	0.16	56	−2.25	0.10
−21.25......	28	−1.95	0.22						
−21.00......	15	−2.04	0.24	6	−2.60	0.24	26	−2.24	0.12
−20.75......	14	−1.84	0.24						
−20.50......	5	−1.90	0.32	5	−2.20	0.22	11	−1.96	0.15
−20.25......	3	−1.00	0.21						

Note.—The SWML binned LFs as a function of absolute magnitude M_K where log n is the logarithm of the comoving density (number/h^{-3} Mpc^3 mag) and σ is its uncertainty. The late-type and early-type LFs were derived using $\Delta M = 0.5$ mag bin widths, twice that for the full sample. The errors for the individual bins are very highly correlated and cannot be used directly if the uncertainty weightings are quantitatively important.

1000 km s^{-1} samples are mutually consistent. Figure 4 shows the likelihood contours for the Schechter function α and M_{K*} parameters as compared to earlier derivations of the infrared LFs. Note that the early-type and late-type LFs have similar shapes, as was also found in the CfA (Marzke et al. 1994a) and SSRS2 (Marzke et al. 1998) morphologically classified LFs. The total LF is steeper than those of the individual types ($\alpha = -1.09 \pm 0.06$ rather than $\alpha = -0.87 \pm 0.09$ or -0.92 ± 01.0) because adding the fainter, more numerous late-type galaxies to the early-type

TABLE 3

2MASS Parametric Luminosity Functions

Name	Type	N	M_{K*} (mag)	α	n_* (10^{-2} h^3 Mpc^{-3})	j (10^8 h $L_\odot$ Mpc^{-3})
Standard	All	3878	-23.39 ± 0.05	-1.09 ± 0.06	1.16 ± 0.10	7.67 ± 0.91
	Late	2097	-22.98 ± 0.06	-0.87 ± 0.09	1.01 ± 0.13	4.06 ± 0.57
	Early	1781	-23.53 ± 0.06	-0.92 ± 0.10	0.45 ± 0.06	3.08 ± 0.49
$cz > 1000$ km s^{-1}	All	4096	-23.35 ± 0.04	-1.02 ± 0.05	1.19 ± 0.10	7.31 ± 0.77
	Late	2244	-23.00 ± 0.05	-0.89 ± 0.07	1.00 ± 0.12	4.11 ± 0.53
	Early	1852	-23.51 ± 0.06	-0.89 ± 0.08	0.46 ± 0.06	3.02 ± 0.44
Bootstrap	Late	...	-23.02 ± 0.06	-0.96 ± 0.09	0.91 ± 0.10	3.84 ± 0.30
	Early	...	-23.52 ± 0.05	-0.90 ± 0.09	0.48 ± 0.04	3.31 ± 0.28
Boundary $T = -1.5$......	Late	2311	-22.98 ± 0.06	-0.87 ± 0.09	1.14 ± 0.14	4.58 ± 0.61
	Early	1567	-23.55 ± 0.07	-0.85 ± 0.11	0.38 ± 0.05	2.56 ± 0.42
Boundary $T = 0.5$	Late	1827	-22.98 ± 0.06	-0.87 ± 0.10	0.88 ± 0.13	3.58 ± 0.53
	Early	2051	-23.52 ± 0.06	-0.99 ± 0.09	0.53 ± 0.06	3.68 ± 0.57
Boundary $T = 1.5$	Late	1472	-23.02 ± 0.07	-0.94 ± 0.10	0.68 ± 0.10	2.91 ± 0.50
	Early	2406	-23.47 ± 0.06	-0.99 ± 0.08	0.66 ± 0.07	4.39 ± 0.63

Note.—The standard model uses a velocity limit $cz > 2000$ km s^{-1}, and the boundary between early-type and late-type galaxies is $T = -0.5$. The "Name" column shows the change made to the standard model to derive that case's parameters. The "Bootstrap" case randomly resamples the galaxies with replacement, including Poisson variations in the number of galaxies and the addition of random errors to the morphological types (see text). Its density uncertainties do not include the contribution from sample variance due to large-scale structure. We present the Schechter function parameters M_{K*}, α, and n_* (eq. [2]) and the local luminosity density j corrected to the total luminosity (see § 4). We use $H_0 = 100\,h$ km s^{-1} Mpc^{-1} in estimating M_{K*}, n_*, and j.

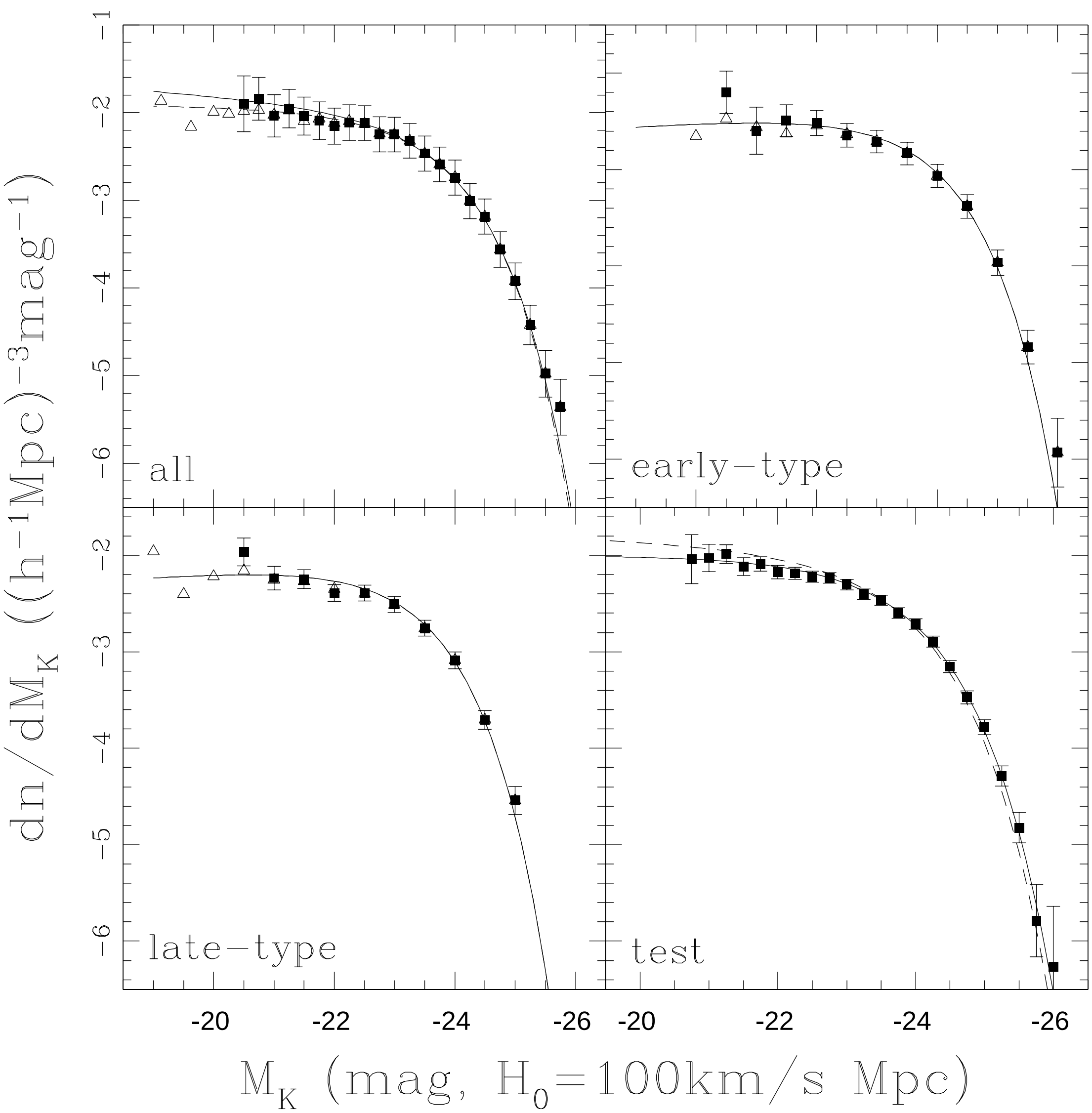

FIG. 3.—LF estimates. The four panels show the fit to the full sample (*top left*), the early-type galaxy subsample (*top right*), the late-type galaxy subsample (*bottom left*), and a Monte Carlo test (*bottom right*). The symbols are the nonparametric SWML model of the LF, and the curves are the best-fit Schechter functions found with the Sandage et al. (1979) method. The filled squares with error bars and the solid line are for the $cz > 2000$ km s^{-1} sample, while the open triangles without error bars and the dashed line are for the $cz > 1000$ km s^{-1} sample. For $M_K \lesssim -21$ mag the symbols for the two samples are superposed. The dashed curve in the Monte Carlo test panel is the input LF, which was chosen to match the best fit to the full sample. The error bars are highly correlated and include the global uncertainty in the density normalization. Only bins containing at least four galaxies are shown.

galaxies makes the summed LF steeper than either of the components. The values of α and M_{K*} are strongly correlated, with a dimensionless covariance of $C_{\alpha M_{K*}}/(C_{\alpha\alpha} C_{M_{K*} M_{K*}})^{1/2} = 0.85$ for all three $cz > 2000$ km s^{-1} LFs, as we would expect from the shapes of the likelihood contours in Figure 4. The uncertainties in the galaxy density have similar contributions from sampling errors and changes correlated with α and M_{K*}.[8]

We also explored the effects of classification errors on the results. We first examined the effects of simple classification errors using Monte Carlo resampling. We randomly selected a new galaxy sample (bootstrap resampling with replacement) including Poisson variations in the total number of galaxies. For each galaxy, we added a 1.8 T-type Gaussian deviate to its classification before dividing the sample into early-type and late-type galaxy subsamples. This random dispersion is a little larger than the 1.6 T-type dispersion between our internal classifications and RC3 but matches the dispersion in the morphological classification experiments conducted by Naim et al. (1995a, 1995b). The results after repeating the process 100 times are summarized in Table 3, where we present the average parameters and their dispersions. These uncertainty estimates will underestimate the uncertainties in the absolute density normalization because they include only the Poisson variance in the expected number of galaxies without the sample variance due to our survey volume and larger scale structure. Aside from the sample variance, the parameter errors and correlations estimated by these bootstrap calculations should be more statistically reliable than those estimated

[8] The value of n_* changes with α and M_{K*} as $n_* = 0.45 - 0.25\,\Delta\alpha + 0.77\,\Delta M_{K*}$ for the early-type galaxies and as $n_* = 1.01 - 0.92\,\Delta\alpha + 2.44\,\Delta M_{K*}$ for the late-type galaxies, where $\Delta\alpha$ and ΔM_{K*} are the changes in α and M_{K*} from the maximum likelihood solutions and n_* is in units of $10^{-2}\,h^3$/Mpc^3.

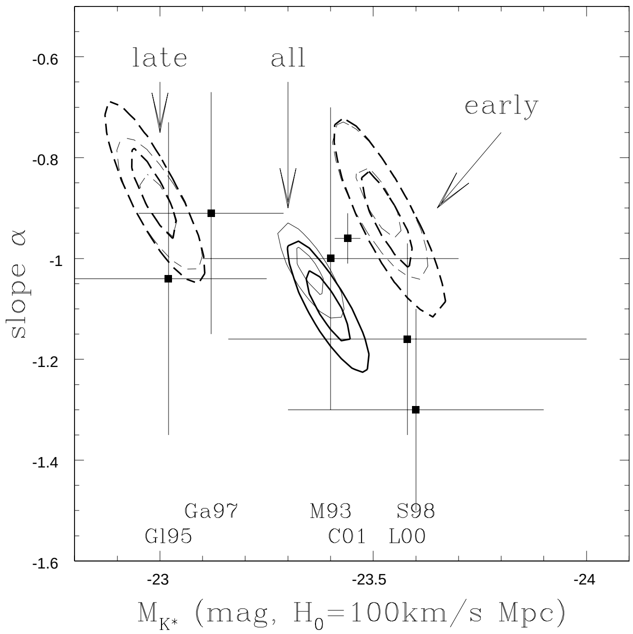

FIG. 4.—Schechter function parameter likelihoods. The 1 and 2 σ likelihood contours for one parameter are shown for the Schechter function parametric fits to the early-type galaxy subsample, the full sample, and the late-type galaxy subsample. The thick contours are for the $cz > 2000$ km s^{-1} sample, and the thin contours are for the $cz > 1000$ km s^{-1} sample. The points with error bars show results from the literature as compiled and standardized by Loveday (2000). The points are, from left to right, Glazebrook et al. (1995, Gl95), Gardner et al. (1997, Ga97), Mobasher et al. (1993, M93), Cole et al. (2001, C01), Loveday (2000, L00), and Szokoly et al. (1998, S98). We estimate that the Cole et al. (2001) point should be shifted by 0.08 ± 0.06 mag to convert their Kron magnitudes to our isophotal magnitudes, bringing the two surveys into excellent agreement.

from the likelihood function. The results are stable to these statistical errors, since the Schechter function parameters and their bootstrap uncertainties are consistent with the simpler maximum likelihood estimates. As we discuss in Kochanek, Pahre, & Falco (2000b), LFs are not stable to even small, random classification uncertainties when the LF shape depends strongly on the type (as is found in spectrally typed LFs like ESP, LCRS, and 2dFGRS).

Next we explored the sensitivity of the results to shifts in the boundary between early-type and late-type galaxies. In our standard LF determination we set the boundary at $T = -0.5$ so that the S0/a galaxies (type $T = 0$) are counted as late-type galaxies. In Table 3 we show the results of shifting the boundary for early-type galaxies to $T \leq -1.5$ (S0 is the first early type), -0.5 (our standard LF, with S0+ as the first early type), 0.5 (S0/a is the first early type), and 1.5 (Sa is the first early type). The parameters M_{K*} and α are insensitive to the boundary shifts, while the comoving density n_* follows the changes in the relative numbers of galaxies.

Figure 4 and Table 4 compare our Schechter parameter estimates to previous results for the total infrared LF from Mobasher et al. (1993), Glazebrook et al. (1995), Gardner et al. (1997), Szokoly et al. (1998), Loveday (2000), and Cole et al. (2001). Aside from Cole et al. (2001), the sample sizes of these surveys are so much smaller that their statistical uncertainties dominate any comparison to our results. Similarly, the uncertainties in the Coma Cluster LF estimates by de Propris et al. (1998) and Andreon & Pello (2000) are significantly larger than for these field surveys. Our results are statistically consistent with all these smaller samples.

The Cole et al. (2001) sample, also of 2MASS galaxies, is approximately 4 times larger and has correspondingly smaller statistical uncertainties. The agreement between our results is significantly better than for any other pair of LF determinations (see § 5). However, although the Schechter function parameters presented in Table 4 appear to be statistically consistent, Figure 4 shows that our solutions are shifted perpendicular to the long axis of the likelihood ellipse leading to a formal disagreement of approximately 3 σ. Although both surveys were based on the 2MASS photometric catalogs, they differ in several respects. First, our sample with $K_s \leq 11.25$ mag is much brighter than the Cole et al. (2001) sample with $K_s \leq 13.20$ mag. Using a magnitude limit further from the catalog magnitude limit of $K_s \simeq 13.5$ mag significantly reduces many sources of systematic errors for photometry, spectral, and cosmological corrections, identifying galaxies and rejecting stars. Second, our redshift survey is complete and includes all the 2MASS galaxies in our survey regions to our magnitude limit, while

TABLE 4
OTHER INFRARED LUMINOSITY FUNCTIONS

Sample	N	M_{K*} (mag)	α	n_* ($10^{-2}\ h^3$ Mpc^{-3})	Type
Mobasher et al. (1993)	181	-23.4 ± 0.3	-1.0 ± 0.3	1.12 ± 0.16	Optical, 100% complete
Glazebrook et al. (1995)......	335	-23.02 ± 0.23	-1.04 ± 0.31	2.90 ± 0.70	Redshift, 37% complete
Gardner et al. (1997)	567	-23.12 ± 0.17	-0.91 ± 0.24	1.66	Redshift, 90% complete
Szokoly et al. (1998)	867	-23.6 ± 0.3	-1.3 ± 0.2	1.2 ± 0.4	Redshift, 31% complete
Loveday (2000)................	345	-23.58 ± 0.42	-1.16 ± 0.19	1.2 ± 0.8	Optical, 100% complete
de Propris et al. (1999)		-23.3 ± 0.7	-0.8 ± 0.4	...	Coma Cluster
Cole et al. (2001)..............	17173	-23.44 ± 0.03	-0.96 ± 0.05	1.08 ± 0.06	Optical, 90% complete
This paper (standard)	3878	-23.39 ± 0.05	-1.09 ± 0.06	1.16 ± 0.10	Redshift, 100% complete

NOTE.—Table derived from Loveday 2000. The "Optical" surveys used K-band imaging of galaxies from an optically selected redshift survey, and the "Redshift" surveys obtained redshifts for objects selected from an infrared imaging survey. de Propris et al. 1999 constructed a volume-limited sample in the Coma Cluster. Mobasher et al. 1993 magnitudes have been adjusted by 0.22 mag as a result of k-correction differences (see Glazebrook et al. 1995; Gardner et al. 1997). An aperture correction of -0.30 is added to the Glazebrook et al. 1995 magnitudes (see Gardner et al. 1997). We show the Glazebrook et al. 1995 results for $z < 0.2$, which includes only 55 galaxies with redshifts. The Cole et al. 2001 value of M_{K*} should be shifted by 0.08 ± 0.06 mag to convert it to our magnitude scale (see Appendix). The Gardner et al. 1997 paper contains no estimate for the uncertainties in n_*. The Poisson uncertainties are $0.07 \times 10^{-2}\ h^3$ Mpc^{-3}, but the true error will be dominated by sample variance due to the finite survey volume. All the results are scaled to $H_0 = 100\ h$ km s^{-1} Mpc^{-1}.

Cole et al. (2001) has redshifts only for the 90% of 2MASS extended sources identified as galaxies in the APM catalog used as the basis for the 2dFGRS survey. Redshifts are lacking if the APM catalog classified the object as a star (4.6% of targets), if the source was an unresolved merger in the APM (4.4% of targets), or if the APM images were of poor quality near the target (0.3% of targets).

Finally, we used different magnitude systems. As we discuss in the Appendix, our sample was selected using K_{20}, the 2MASS magnitude *k_m_k20fc* inside the circular isophote corresponding to a surface brightness of $\mu_{K_s} = 20$ mag arcsec^{-2}. The Cole et al. (2001) sample used $K_{\rm Kron}$, the 2MASS Kron magnitude *k_m_e*. For our magnitude range the difference between the two magnitudes is negligible ($\langle K_{\rm Kron} - K_{20} \rangle = -0.01$ mag with a scatter of 0.09 mag; see Appendix), while for the fainter Cole et al. (2001) sample there is a small mean offset. We estimate that the K_{20} isophotal magnitudes are offset by -0.20 ± 0.04 mag from the total magnitudes, while Cole et al. (2001) estimate that their $K_{\rm Kron}$ magnitudes are offset by -0.12 ± 0.05 mag from the total magnitudes. These offsets indicate that we should shift the Cole et al. (2001) magnitudes by 0.08 ± 0.06 mag to compare them to our magnitudes. This shift from their Kron $M_{K*} = -23.44 \pm 0.03$ to our K_{20} $M_{K*} = -23.36 \pm 0.07$ is sufficient to explain the differences in the Schechter function parameters.

4. THE LOCAL INFRARED LUMINOSITY DENSITY

Estimates of the total mass density in stars are almost always based on *B*-band LFs and mass-to-light ratios (for recent estimates see Fukugita, Hogan, & Peebles 1998). Since the blue luminosity is dominated by young, massive stars and strongly affected by dust extinction, using the blue luminosity density to estimate the stellar mass density introduces enormous systematic uncertainties independent of any shortcomings in the LFs. The *K*-band luminosity density avoids most of these problems since the infrared luminosity is less dominated by massive stars and even dusty local galaxies are nearly transparent at *K* band. We compute the luminosity density by integrating over the Schechter function fits to the data, $j = L_* n_* \Gamma(2 + \alpha)$, using a *K*-band magnitude zero point of $M_{\odot,K_s} = 3.39$ mag (Johnson 1966). We must also correct our isophotal luminosities to the total luminosity, which adds a correction factor of $f = 1.21 \pm 0.04$ to the luminosity density, $j = f L_* n_* \Gamma(2 + \alpha)$ estimated from our Schechter function parameters (see Appendix). While we found the same correction factor for both early-type and late-type galaxies, we will be conservative and assume that the uncertainties in the correction are statistically independent. We will write the luminosity density as $j = j_8 10^8\ h\ L_\odot$ Mpc^{-3} to compress the notation.

Table 3 presents the luminosity density estimated for each LF. Note that the luminosity density estimated by fitting the sample with a single LF is systematically higher than that obtained by summing the luminosity densities of the two galaxy types. For example, in our standard model we find $j_8 = 7.67 \pm 0.91$ using the global LF but $j_8 = 7.14 \pm 0.75$ from the sum of the early-type and late-type luminosity densities. The $\Delta v > 1000$ km s^{-1} sample shows a similar but smaller difference ($j_8 = 7.31 \pm 0.77$ vs. 7.13 ± 0.69). The offset is probably a systematic effect created by the steeper slopes (α) found for the total LF as compared to the LFs by type. The effect is smaller for the $\Delta v > 1000$ km s^{-1} sample because the faint-end slope of the total LF is shallower. When we sum the luminosity densities for the early- and late-type galaxies, we find that the total luminosity density is little affected by classification uncertainties or the location of the type boundary. For example, we found the same luminosity density in the bootstrap resampled model ($j_8 = 7.15 \pm 0.38$) as we found in the standard model. The luminosity density of the late-type galaxies slightly exceeds that of the early-type galaxies, with $j_{\rm late}/j_{\rm early} = 1.17 \pm 0.13$ when we include both the classification uncertainties and the independent magnitude calibration uncertainties for the two types. The ratio varies rapidly as we change the type boundary, with ratios of $j_{\rm late}/j_{\rm early} = 1.79$, 1.31, 0.97, and 0.68 for boundaries at $T = -1.5$, -0.5 (the standard model rather than the bootstrap model), 0.5, and 1.5, respectively. The early-type spiral galaxies dominate the contribution of the late-type galaxies to the luminosity density.

Our results agree with the luminosity density estimates of Cole et al. (2001). Their raw luminosity density of $j_8 = 5.74 \pm 0.32$ becomes $j_8 = 6.41 \pm 0.46$ after adding their correction factor of $f = 1.12 \pm 0.05$ for the difference between their Kron survey magnitudes and the total magnitudes. This value is slightly lower but consistent with our best estimate of $j_8 = 7.14 \pm 0.75$. Since Cole et al. (2001) found a shallower faint-end slope than in our standard model (see Fig. 4), they would not find a significant difference between estimates of j using a global LF as compared to the sum of the estimates for each galaxy type.

Finally, we can use the luminosity density to estimate the stellar density in units of the critical density, $\Omega_* h = 0.00036 \langle M/L \rangle j_8$, where $\langle M/L \rangle$ is the average *K*-band mass-to-light ratio. Cole et al. (2001) estimated average *K*-band mass-to-light ratios of 0.73 $M_\odot/L_\odot$ for a Kennicutt IMF and 1.32 $M_\odot/L_\odot$ for a Salpeter IMF including only stars above 0.1 $M_\odot$. For our standard model this implies $\Omega_* h = (1.9 \pm 0.2) \times 10^{-3}$ for the Kennicutt IMF and $\Omega_* h = (3.4 \pm 0.4) \times 10^{-3}$ for the Salpeter IMF. The densities are 10% higher than the Cole et al. (2001) estimates because of our slightly higher luminosity densities and are consistent with the Fukugita et al. (1998) best estimate of $\Omega_* h = 2.5 \times 10^{-3}$ with a range of $1.4 \times 10^{-3} < \Omega_* h < 4.0 \times 10^{-3}$.

5. COMPARISON TO OPTICAL LUMINOSITY FUNCTIONS

Our infrared LFs are the first large enough to compare directly to the results of recent estimates of the LF from optical redshift surveys, many of which are summarized in Table 5. The optical LFs, particularly those divided by galaxy type, show inconsistencies in their magnitude scales, shapes, and density normalizations that are significantly larger than their formal uncertainties. In Kochanek et al. (2000a) we show that the LFs defined by spectral types using small-aperture fiber spectrographs (LCRS, ESP, and by extension 2dFGRS and SDSS) have internally inconsistent type definitions that can severely bias the shapes of the derived LFs. In essence, the small spectral apertures sample a varying fraction of the bulge and the disk of spiral galaxies, leading to flux- and luminosity-dependent biases between the true and measured spectral types of the galaxies. Local, bright, morphologically typed surveys (e.g., this sample, CfA, and SSRS2) and large-aperture spectrally typed surveys (APM survey by spectral type) appear to have self-consistent type definitions and similarly shaped LFs for

TABLE 5

OPTICAL LUMINOSITY FUNCTIONS

Survey	Type	N	Band	M_* (mag)	$\langle m - K_{20} \rangle$ (mag)	α	n_* ($10^{-2}\ h^3\ \mathrm{Mpc}^{-3}$)	Reference
APM	All	1658	B_J	-19.50 ± 0.13	3.39 ± 0.62	-0.97 ± 0.15	1.40 ± 0.17	1
	Early	311		-19.71 ± 0.25	3.73 ± 0.47	0.20 ± 0.35	...	1
	Late	999		-19.40 ± 0.16	3.25 ± 0.68	-0.80 ± 0.20	...	1
Century	All	1762	R_C	-20.73 ± 0.18	...	-1.17 ± 0.19	2.50 ± 0.60	2
CfA	All	9063	B_Z	-18.80 ± 0.30	3.46 ± 0.89	-1.00 ± 0.20	4.00 ± 1.00	3
	E			-19.23 ± 0.2	4.10 ± 0.65	-0.85 ± 0.20	0.15 ± 0.04	4
	S0			-18.74 ± 0.1	3.95 ± 0.65	-0.94 ± 0.15	0.76 ± 0.20	4
	Sa/b			-18.72 ± 0.1	3.79 ± 0.56	-0.58 ± 0.15	0.87 ± 0.22	4
	Sc/d			-18.81 ± 0.2	3.34 ± 0.64	-0.96 ± 0.15	0.44 ± 0.11	4
	Sm/Im			-18.79 ± 0.5	2.40 ± 0.73	-1.87 ± 0.20	0.06 ± 0.02	4
ESP	All	3342	B_J	-19.61 ± 0.08	...	-1.22 ± 0.07	2.00 ± 0.4	5
	em	1575		-19.47 ± 0.10	...	-1.40 ± 0.10	1.00 ± 0.2	5
	Not-em	1767		-19.62 ± 0.10	...	-0.98 ± 0.09	1.10 ± 0.2	5
LCRS	All	18678	R_C	-20.29 ± 0.02	2.43 ± 0.28	-0.70 ± 0.03	1.90 ± 0.1	6
	Not-em	11366		-20.22 ± 0.02	2.48 ± 0.21	-0.27 ± 0.04	1.10 ± 0.1	6
	em	7312		-20.03 ± 0.03	2.32 ± 0.35	-0.90 ± 0.04	1.30 ± 0.1	6
	1	655		-20.28 ± 0.07	2.54 ± 0.17	0.54 ± 0.14	0.034 ± 0.003	7
	2	7614		-20.23 ± 0.03	2.50 ± 0.18	-0.12 ± 0.05	0.71 ± 0.06	7
	3	4667		-19.90 ± 0.04	2.44 ± 0.26	-0.32 ± 0.07	0.99 ± 0.13	7
	4	3210		-19.85 ± 0.05	2.33 ± 0.32	-0.64 ± 0.08	1.15 ± 0.21	7
	5	1443		-20.03 ± 0.09	2.18 ± 0.34	-1.33 ± 0.09	0.84 ± 0.22	7
	6	689		-20.01 ± 0.14	1.89 ± 0.38	-1.84 ± 0.11	1.31 ± 0.78	7
SSRS2	All	5036	$B(0)$	-19.43 ± 0.06	3.55 ± 0.83	-1.12 ± 0.05	1.28 ± 0.20	8
	E/S0	1587		-19.37 ± 0.11	4.07 ± 0.58	-1.00 ± 0.09	0.44 ± 0.08	8
	Spiral	3227		-19.43 ± 0.08	3.32 ± 0.81	-1.11 ± 0.07	0.80 ± 0.14	8
	Irr/pec	204		-19.78 ± 0.45	3.22 ± 1.04	-1.81 ± 0.24	0.20 ± 0.08	8
2dFGRS	All	5869	B_J	-19.73 ± 0.06	...	-1.28 ± 0.05	1.69 ± 0.17	9
	1	1850		-19.61 ± 0.09	...	-0.74 ± 0.11	0.90 ± 0.09	9
	2	928		-19.68 ± 0.14	...	-0.86 ± 0.15	0.39 ± 0.06	9
	3	1200		-19.38 ± 0.12	...	-0.99 ± 0.13	0.53 ± 0.08	9
	4	1193		-19.00 ± 0.12	...	-1.21 ± 0.12	0.65 ± 0.13	9
	5	668		-19.02 ± 0.22	...	-1.73 ± 0.16	0.21 ± 0.11	9

NOTE.—For the color difference $\langle m - K_{20} \rangle$ we give the mean color and the dispersion in the color. The statistical uncertainty in the mean color is generally less than 0.05 mag, and the mean color was calculated over a magnitude range such that the survey magnitude limits would not affect the colors. We cannot calculate $\langle m - K_{20} \rangle$ for the ESP (too little overlap with the current 2MASS catalog), Century (no published object lists), and 2dFGRS (no published object lists) surveys.

REFERENCES.—(1) Loveday et al. 1992. (2) Geller et al. 1997. (3) Marzke et al. 1994b. (4) Marzke et al. 1994a. (5) Zucca et al. 1997. (6) Lin et al. 1996. (7) Bromley et al. 1998. (8) Marzke et al. 1998. (9) Folkes et al. 1999.

both early- and late-type galaxies. Differences in the surface brightness selection effects of the surveys can also lead to differences in the shapes of the LFs (e.g., Disney 1976; Huchra 1999; Cross et al. 2001).

The luminosity scales (L_* or M_*) of the optical surveys differ by more than can be explained by any statistical uncertainties even after including the strong covariances between α and M_* in Schechter function models of the LF. For example, the value of M_* found for the CfA survey (Marzke et al. 1994a, 1994b) is 0.75 mag fainter than the other blue-selected surveys (APM, ESP, SSRS2, and 2dFGRS). The current 2MASS catalogs overlap many of the optical surveys, which allows us to calculate the extinction and k-corrected average "color" $\langle m - K_{20} \rangle$ between the optical survey and the 2MASS survey. This "color" includes both the true color difference of the galaxies and terms due to the different apertures used by the surveys to define their magnitudes. Since the intrinsic colors and the 2MASS magnitudes do not depend on the properties of the optical surveys, we can use the color differences between the surveys to test for differences in magnitude definitions and type assignments. We can estimate the average colors for the APM, CfA, LCRS, and SSRS2 surveys, and we present the results in Table 5. As we would expect, later type galaxies are bluer than early-type galaxies, but the color differences can be significantly smaller than the width of the color distribution. For example, the LCRS emission-line and non–emission-line samples (Lin et al. 1996) have a color difference of only 0.15 mag but a much larger dispersion in the colors of each type. The depth of the 2MASS survey is not well matched to that of the LCRS survey, so our color estimate is dominated by the bright LCRS galaxies (the 2MASS galaxy magnitude limit of $K_s \simeq 13.5$ mag corresponds to $R_C \simeq 16$ mag, while the LCRS survey is over the range $R_C = 15$–18 mag). The minimal color differences are probably a symptom of the aperture biases affecting the LCRS spectral classifications, in which bright late-type galaxies are misclassified as early-type galaxies (see Kochanek et al. 2000a). The mismatch of the color differences between types and the color dispersion for the individual types becomes larger when the sample is divided more finely using the spectral clan classification of the LCRS galaxies by Bromley et al. (1998).

The colors do not provide a simple explanation for the M_* differences between the various surveys. For example, $\langle B-K \rangle \simeq 3.45 \pm 0.07$ mag for the APM (B_J magnitudes), CfA (B_Z Zwicky magnitudes), and SSRS2 [$B(0)$ magnitudes] surveys even though the characteristic magnitude of the CfA survey is 0.7 mag fainter than the APM and SSRS2 surveys. The colors of the early-type galaxies in the CfA and SSRS2 surveys are very similar, while their colors in the APM survey are 0.3 mag bluer. This is consistent with the incompleteness in the APM morphological classifications being dominated by the more distant, red early-type galaxies (see Loveday et al. 1992; Marzke et al. 1994a). With the exception of the Sa/Sb galaxies in the CfA survey, which are relatively red and have an anomalous value for α, the late-type galaxies in the three surveys have very similar colors.

6. COMPARISONS TO THE PROPERTIES OF FAINT INFRARED SAMPLES

One important use of local LFs is in estimates of the properties of fainter or higher redshift galaxies. Here we make some comparisons to the magnitude and redshift distributions of fainter infrared galaxies using simple evolution models. We combined our LFs with Bruzual & Charlot (1993, GISSEL96 version) galaxy evolution models assuming an $\Omega_0 = 0.3$ flat cosmological model and $H_0 = 65$ km s^{-1} Mpc^{-1} to determine the distances and ages. We considered no evolution models (k-corrections only) and evolving models using an "Sb" template for the late-type galaxies (based on the star formation history models of Guiderdoni & Rocca-Volmerange 1988) and a 1 Gyr exponential burst (SFR $\propto \exp[-(t - t_f)/\mathrm{Gyr}]$) for the early-type galaxies where the populations formed at $z_f = 3$ or 5. We predicted the number counts and redshift distributions of galaxies as a function of magnitude and compared them to the available observational data. All the models are consistent with the number counts and redshift distributions measured for our low-redshift sample (see Figs. 5 and 6), confirming that we have derived LFs consistent with our data. Table 6 presents the number counts for our current sample.

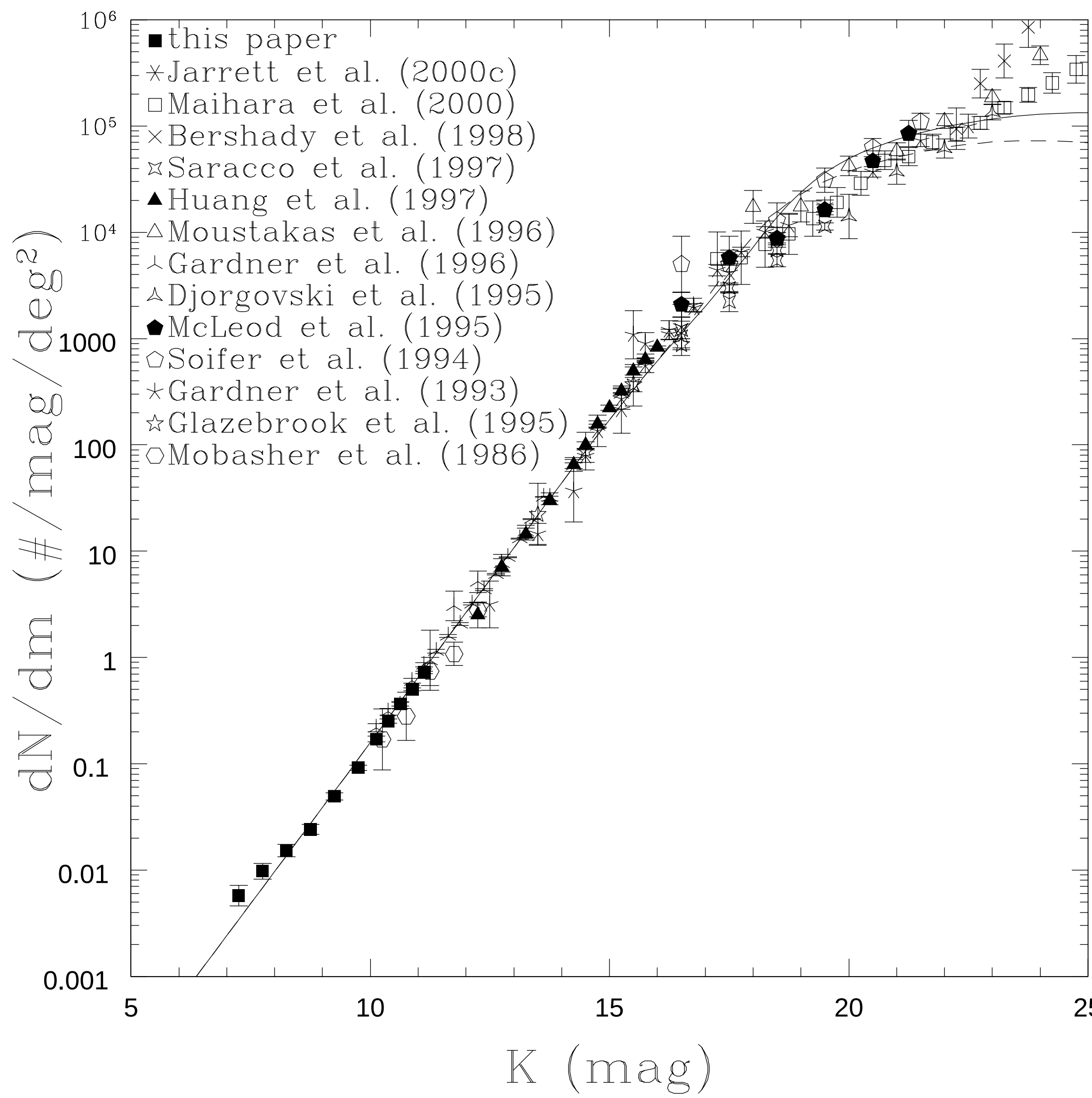

FIG. 5.—Differential K-band galaxy number counts. The points show the results of a wide range of surveys including the number counts of our sample. The solid (dashed) curve shows the predictions for a formation epoch of $z_f = 5$ ($z_f = 3$). Our local counts and LFs use K_s-band isophotal magnitudes (see § 2). We made no corrections for the differences between the K, K_s, and K' filters and made no attempt to standardize the definitions of the galaxy magnitudes. References: Jarrett et al. (2000a); Maihara et al. (2000); Bershady et al. (1998); Saracco et al. (1997); Huang et al. (1997); Moustakas et al. (1997); Gardner et al. (1996); Djorgovski et al. (1995); McLeod et al. (1995); Soifer et al. (1994); Gardner et al. (1993); Glazebrook et al. (1995); Mobasher et al. (1986).

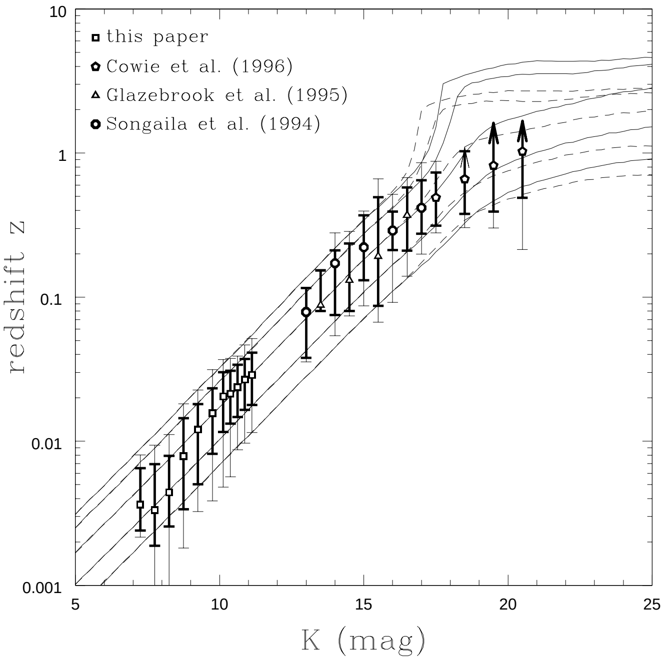

FIG. 6.—Redshift distributions predicted by pure luminosity evolution models. The solid (dashed) curves are contours of the redshift distribution for formation epochs of $z_f = 5$ ($z_f = 3$). From top to bottom, 95%, 84% (1 σ above the median), 50% (the median), 16% (1 σ below the median), and 5% of galaxies are predicted to have lower redshifts than the corresponding curve. The symbols and error bars show the distributions observed in our sample and the fainter samples of Songaila et al. (1994), Glazebrook et al. (1995), and Cowie et al. (1996). The symbols correspond to the sample median at each magnitude, the thick error bars span the 1 σ region (16%–84% of the sorted sample), and the thin error bars span the 5%–95% region. To construct the sample statistics, unobserved objects were assumed to have the median redshift, and objects with unmeasured redshifts were assumed to lie at high redshift. An arrow indicates that the upper limit would be due to the objects with unmeasured, but assumed to be high, redshifts, with the tip of the arrow located at the highest measured redshift.

It is no surprise that no evolution models with a finite formation epoch are unable to reproduce either the number counts or the redshift distributions. The predicted counts lie below the observations and the predicted redshifts are systematically lower than observed once $K \gtrsim 16$ mag. Particularly for early-type galaxies, there is direct evidence that the infrared luminosities evolve significantly by redshift unity. Pahre, Djorgovski, & de Carvalho (1999) used the fundamental plane to measure the amount of surface brightness evolution of cluster early-type galaxies to $z \simeq 0.5$, de Propris et al. (1999) measured the evolution of the cluster LFs to $z \simeq 1$, and Kochanek et al. (2000a) used the fundamental plane of gravitational lenses to measure the surface brightness evolution of field early-type galaxies to $z \simeq 1$. All three estimates require stellar populations formed in short bursts at $z_f = 2$–5 rather than no evolution models.

Pure luminosity evolution models, where the comoving numbers of galaxies are fixed but the stellar populations are allowed to evolve, work far better. Figures 5 and 6 show that populations formed at $z_f = 3$ or 5 are relatively consistent with both the number counts and the redshift distributions for $K \lesssim 18$ mag. At fainter magnitudes these models begin to have too low a surface density and too high an average redshift. The high-redshift tail in the distribution is due to the $z \gtrsim 1$ early-type galaxies, which are predicted to be very luminous. Kauffmann & Charlot (1998) use this disagreement and their semianalytic models of galaxy formation to argue that many L_* early-type galaxies must be formed from mergers occurring near redshift unity. Indeed, crude merger models with $n_* \propto (1 + z)^\gamma$, $L_* \propto 1/n_*$ to conserve the total mass and $\gamma \simeq 1$ naturally eliminate the high-redshift tail and increase the number counts of faint galaxies.

Unfortunately, the differences between the predicted and observed redshift distributions may also be due to sample variance rather than rapid merging. We can see the effects of sample variance in Figure 6 both at $z \lesssim 0.01$ for our sample and in the differences between the redshift distributions found by Glazebrook et al. (1995) and Songaila et al. (1994) at similar apparent magnitudes. While the differences in the survey geometries (equal axes vs. pencil beam) mean that large-scale structure affects the survey statistics differently, our comoving volume out to $z = 0.01$ is 30 times larger than the survey volume of the Cowie et al. (1996) fields out to redshift unity. If we link galaxies in the Cowie et al. (1996) fields with velocity differences smaller than 1000 km s^{-1} into single "objects" (to try to suppress the effects of correlated structures on the redshift distribution), the median redshift increases significantly (by $\Delta z \simeq 0.2$). Thus, significantly larger redshift samples are needed to test evolutionary models quantitatively.

TABLE 6

DIFFERENTIAL K_s-BAND NUMBER COUNTS

K_s (mag)	ΔK_s (mag)	N	log (dN/dm) (number mag^{-1} deg^{-2})	Poisson Errors
7.250	0.50	20	−2.24	0.097
7.750	0.50	36	−2.01	0.074
8.250	0.50	53	−1.82	0.060
8.750	0.50	84	−1.62	0.047
9.250	0.50	172	−1.31	0.033
9.750	0.50	320	−1.04	0.024
10.125	0.25	298	−0.766	0.025
10.375	0.25	439	−0.598	0.021
10.625	0.25	635	−0.438	0.017
10.875	0.25	872	−0.300	0.015
11.125	0.25	1263	−0.141	0.012

NOTE.—There are N galaxies in each bin centered at K_s and of width ΔK_s, corresponding to number counts of dN/dm in mag^{-1} deg^{-2} and its corresponding Poisson uncertainty. These are the 2MASS $\mu_{K_s} = 20$ mag arcsec^{-2} circular isophotal magnitudes (Jarrett et al. 2000a).

7. SUMMARY

We have derived the first local infrared galaxy sample divided by galaxy type whose statistical uncertainties are comparable to those of local optical galaxy LFs. We derived both total and morphologically typed LFs. Our morphological types are self-consistent (see Kochanek et al. 2000a), our LFs are insensitive to random errors in the classifications, and the parameters change as expected when we shift the boundary between early- and late-type galaxies. We find a local K-band luminosity density of $j = (7.14 \pm 0.75) \times 10^8\, h\, L_\odot$ Mpc^{-3}, which implies a stellar mass density relative to critical of $\Omega_* h = (1.9 \pm 0.2) \times 10^{-3}$ for a Kennicutt IMF and $\Omega_* h = (3.4 \pm 0.4) \times 10^{-3}$ for a Salpeter IMF. The luminosity density of late-type galaxies is slightly higher than that of early-type galaxies, with $j_{\rm late}/j_{\rm early} = 1.17 \pm 0.12$. Our total LF, luminosity density, and estimate of Ω_* all agree with the results from Cole et al. (2001) based on a fainter and incomplete but larger sample of 2MASS galaxies selected from the regions surveyed as part of the 2dFGRS redshift survey. While our survey has larger statistical errors than Cole et al. (2001), it should have significantly smaller systematic errors.

Like morphologically typed optical surveys (CfA and SSRS2), we find that the LFs of early- and late-type galaxies have similar shapes, $\alpha \simeq -0.9 \pm 0.1$, in marked contrast to spectrally typed optical surveys (ESO Slice, LCRS, 2dFGRS), which usually find that the slope steepens for late-type galaxies. Note, however, that in Kochanek et al. (2000a) we find that the spectral classification methods are not self-consistent because of the aperture bias created by using a spectroscopic aperture that is much smaller than the galaxies being observed. We used galaxies found in both the optical redshift surveys and the 2MASS survey to estimate the magnitude differences between 2MASS and the optical surveys and also between the different optical surveys. In all surveys, later type galaxies have bluer optical-to-infrared colors, but the magnitude differences cannot fully explain the discrepancies between the magnitude scales of the LFs. Our LFs successfully predict the properties of fainter infrared samples until $K \gtrsim 18$ mag where the models have a significant dependence on galaxy evolution and merging histories and the comparison data are probably affected by sample variance.

These results are preliminary, and the sample is still growing rapidly. In particular, the survey area complete to the current magnitude limit continues to expand rapidly, and it is easy to build complete, deeper samples in restricted areas to extend to fainter absolute magnitude limits. With complete sky coverage we can use the 2MASS catalog to probe the relative completeness of redshift surveys and to improve our comparisons between the survey magnitude scales. By combining this with the surface photometry available for 2MASS galaxies, we can quantitatively explore the effects of surface brightness selection effects (e.g., Disney 1976; Sprayberry et al. 1997; Dalcanton et al. 1997; Huchra 1999; Cross et al. 2001; Blanton et al. 2001) on large redshift surveys. As the coverage gaps are eliminated, we can look at density dependences to galaxy properties. In M. A. Pahre, C. S. Kochanek, & E. E. Falco (2001, in preparation) we derive an improved galaxy velocity function ($dn/d \log v$ instead of dn/dM) based on the Tully-Fisher and Faber-Jackson relations derived from the same 2MASS photometry used to derive the LF. The velocity function is useful because it determines the optical depth of the universe to gravitational lensing (see Falco, Kochanek, & Munoz 1998) and can be used to probe the evolution of galaxies (see Gonzalez et al. 2000).

This research was supported by the Smithsonian Institution. The authors thank P. Berlind and M. Calkins, the FLWO remote observers, for obtaining the redshift data, and S. Tokarz for the data reduction. The 2MASS project is supported by NSF and NASA, and we thank the other members of the 2MASS collaboration for their efforts. We especially thank Susan Kleinmann for her efforts to start the project. We thank J. Loveday for his compilation of infrared LF estimates. M. A. P. was supported by Hubble Fellowship grant HF-01099.01-97A from STScI (which is operated by AURA under NASA contract NAS5-26555).

APPENDIX

THE 2MASS CATALOG AND MAGNITUDES

Our redshift survey simply uses the photometric catalog of extended sources produced by the 2MASS survey. The algorithms for selecting extended sources and estimating their fluxes are detailed in Jarrett et al. (2000a), which includes extensive discussions of the algorithms for separating stars from galaxies and for detecting low surface brightness galaxies and galaxies with starlike cores. Our limiting magnitude of $K_{20} \leq 11.25$ mag is so much brighter than the limiting magnitude of the catalogs, $K_{20} \simeq 13.5$, that confusion and completeness are not an issue for our sample. The pipeline has little difficulty finding "typical" low surface brightness galaxies even at the catalog limit, so the surface brightness biases of our sample should be no worse than the large optical redshift surveys. The only significant problem in constructing our catalog is that the survey supplies an "extended source" catalog from which we must remove extended sources that are not in fact galaxies (see § 2).

For each galaxy, the 2MASS survey estimates a wide variety of magnitudes. We chose to select our targets based on the "default K magnitude" k_m, which for our magnitude range corresponds to the magnitude *k_m_k20fc* inside the circular isophote corresponding to a surface brightness of $\mu_{K_s} = 20$ mag arcsec^{-2}. We call this magnitude K_{20} in the text. The magnitude choice must balance two issues. The primary requirement is to produce a well-defined catalog. The secondary requirement is for a magnitude that is closely related to physically interesting quantities like the total luminosity. We selected K_{20} as our survey magnitude to satisfy the primary requirement, since for our sample it is very well defined, observationally repeatable, and has negligible uncertainties (median errors of 0.03 mag confirmed by repeated scans of several areas on well-separated nights; see T. Jarrett et al. 2000, in preparation). While a fainter isophotal magnitude is available (to $\mu_{K_s} = 21$ mag arcsec^{-2}), it is significantly noisier. The elliptical isophotal magnitudes give slightly more accurate flux estimates unless stellar contamination skews the parameters of the ellipse (see Jarrett et al. 2000a). Thus, the choice of circular isophotal magnitudes rather than the elliptical isophotal magnitude emphasizes robustness slightly more than accuracy.

In addition to isophotal magnitudes, the catalog also includes a wide range of fixed aperture magnitudes, Kron (1980) magnitudes, and estimated total magnitudes. We can immediately reject any fixed aperture magnitude, as our sample includes galaxies with $\mu_{K_s} = 20$ mag arcsec^{-2} isophotal radii from 8".0 to 100".0: large apertures would be too noisy for small galaxies, and small apertures would miss most of the flux for large galaxies. We can also reject the estimated total magnitudes because the flux extrapolation is truncated at 80".0, leading to a kink in the relationship between the isophotal magnitude and the estimated total magnitude near $K_{20} = 10$ mag. Kron magnitudes, the final possibility, are almost indistinguishable from the K_{20} isophotal magnitudes in our magnitude range. The average offset between the elliptical aperture Kron magnitude (*k_m_e*) and K_{20} is only -0.01 mag with a dispersion of 0.09 mag. For early-type galaxies the offset is 0.03 mag with a scatter of 0.05

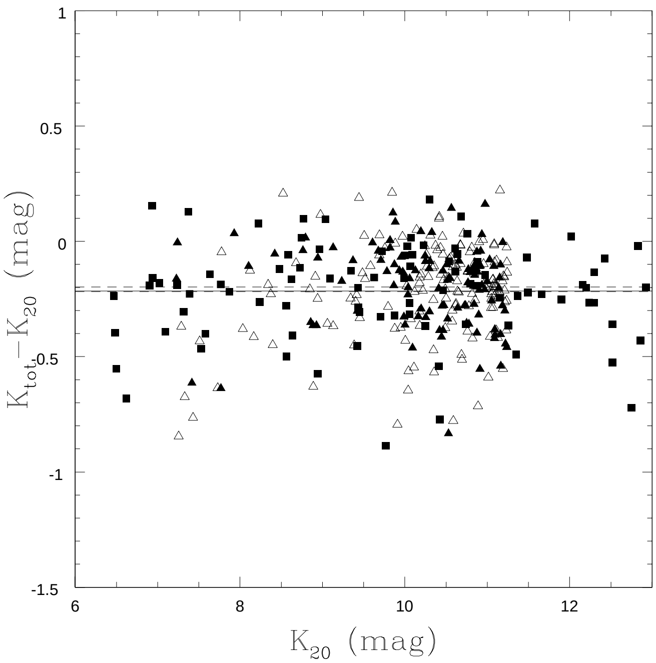

FIG. 7.—Comparison of total and isophotal magnitudes for the early-type galaxies from Pahre (1999; *squares*), the early-type galaxies from Gavazzi et al. (2000; *filled triangles*), and the late-type galaxies from Gavazzi et al. (2000; *open triangles*). The average offsets are shown by the solid line for the Pahre (1999) galaxies and the (overlapping) dashed lines for the two samples from Gavazzi et al. (2000). The dispersions about the relations are approximately 0.20 mag, while we would expect a dispersion of approximately 0.1 mag based on the formal errors.

mag, while for late-type galaxies the offset is -0.04 mag with a scatter of 0.10 mag. The offset for late-type galaxies is reduced to -0.02 mag for the circular aperture Kron magnitudes (*k_m_c*). There is a small slope to the relation, $-0.01(K_{20} - 11.25)$ mag, which would be a negligible correction for most of the sample. Thus, using Kron magnitudes would have little effect on the full sample and would reduce the magnitude difference between early- and late-type galaxies by approximately 0.07 mag or about half of the statistical uncertainties in the M_{K*} parameter of the LF. In general, however, the K_{20} magnitude appears to be the best compromise between precision, robustness, and simplicity.

For quantities like the luminosity density we need to convert our survey magnitudes into total magnitudes. We can examine the relationship between K_{20} and the total luminosity using the sample of early-type galaxies with deep K_s-band photometry from Pahre (1999) and the larger sample of galaxies with deep H-band photometry by Gavazzi et al. (2000) (see Fig. 7). We found 88 early-type Pahre (1999) galaxies in the 2MASS catalog, and our current sample includes 108 early-type and 150 late-type galaxies from the Gavazzi et al. (2000) catalog. We estimated the K_s-band total magnitude by $K_{tot} = H_{tot} + (K-H)_{20}$ using the Gavazzi et al. (2000) estimate for H_{tot} and the 2MASS $H-K$ color inside the isophote defining the K_{20} magnitudes. The average offsets for the three samples are -0.22 ± 0.02, -0.21 ± 0.02, and -0.21 ± 0.02, respectively, with a scatter of 0.20 mag about the mean offset after performing a $3-\sigma$ clipping of the sample to remove gross outliers. There is no statistically significant evidence for a slope in the offset or for a difference in the offsets for early-type and late-type galaxies. The scatter is significantly larger than the 0.10 mag scatter expected from the formal errors on the 2MASS and total magnitudes. The offsets are little affected by the $3-\sigma$ clipping procedure. Given these results, we adopted an offset of $\Delta = -0.20 \pm 0.04$ mag as our correction between the total and isophotal absolute magnitudes. We have taken a very conservative approach and doubled the formal uncertainties. This is consistent with the estimate by Jarrett et al. (2000a) that the K_{20} magnitudes should underestimate the total luminosity by 10%–20%, and we have doubled the formal uncertainties.

REFERENCES

Andreon, S., & Pello, R. 2000, A&A, 353, 479
Bershady, M. A., Lowenthal, J. D., & Koo, D. C. 1998, ApJ, 505, 50
Blanton, M. R., et al. 2001, AJ, 121, 2358
Bromley, B. C., Press, W. H., Lin, H., & Kirshner, R. P. 1998, ApJ, 505, 25
Bruzual, A. G., & Charlot, S. 1993, ApJ, 405, 538
Cardelli, J. A., Clayton, G. C., & Mathis, J. S. 1989, ApJ, 345, 245
Cole, S., et al. 2001, MNRAS, 326, 255
Cowie, L. L., Gardner, J. P., Hu, E. M., Songaila, A., Hodapp, K.-W., & Wainscoat, R. J. 1994, ApJ, 434, 114
Cowie, L. L., Songaila, A., Hu, E. M., & Cohen, J. G. 1996, AJ, 112, 839
Cross, N., et al. 2001, MNRAS, 324, 825
da Costa, L. N., et al. 1994, ApJ, 424, L1
———. 1998, AJ, 116, 1
Dalcanton, J. J., Spergel, D. N., Gunn, J. E., Schmidt, M., & Schneider, D. P. 1997, AJ, 114, 635
Davis, M., & Huchra, J. 1982, ApJ, 254, 437
de Lapparent, V., Geller, M. J., & Huchra, J. P. 1988, ApJ, 332, 44
de Propris, R. D., Eisenhardt, P. R., Stanford, S. A., & Dickinson, M. 1998, ApJ, 503, L45
de Propris, R. D., Stanford, S. A., Eisenhardt, P. R., Dickinson, M., & Elston, R. 1999, AJ, 118, 719
de Vaucouleurs, G., de Vaucouleurs, A., & Crowin, H. G. 1976, Second Reference Catalogue of Bright Galaxies (Austin: Univ. Texas Press)
Disney, M. 1976, Nature, 263, 573
Djorgovski, S., et al. 1995, ApJ, 438, L13
Dressler, A. 1980, ApJ, 236, 351
Efstathiou, G., Ellis, G., & Peterson, B. A. 1988, MNRAS, 232, 431
Fabricant, D., Cheimets, P., Caldwell, N., & Geary, J. 1998, PASP, 110, 79
Falco, E. E., et al. 1999, PASP, 111, 438
Falco, E. E., Kochanek, C. S., & Munoz, J. A. 1998, ApJ, 494, 47
Folkes, S., et al. 1999, MNRAS, 308, 459
Fukugita, M., Hogan, C. J., & Peebles, P. J. E. 1998, ApJ, 503, 518

Gardner, J. P., Cowie, L. L., & Wainscoat, R. J. 1993, ApJ, 415, L9
Gardner, J. P., Sharples, R. M., Carrasco, B. E., & Frenk, C. S. 1996, MNRAS, 282, L1
Gardner, J. P., Sharples, R. M., Frenk, C. S., & Carrasco, B. E. 1997, ApJ, 480, L99
Gavazzi, G., Franzetti, P., Scodeggio, M., Bosellli, A., & Pierini, D. 2000, A&A, 361, 863
Gavazzi, G., Pierini, D., & Bosellli, A. 1996, A&A, 312, 397
Geller, M., et al. 1997, AJ, 114, 2205
Geller, M., & Huchra, J. P. 1989, Science, 246, 897
Glazebrook, K., Peacock, J. A., Collins, C. A., & Miller, L. 1994, MNRAS, 266, 65
Glazebrook, K., Peacock, J. A., Miller, L., & Collins, C. A. 1995, MNRAS, 275, 169
Gonzalez, A. H., Williams, K. A., Bullock, J. S., Kolatt, T. S., & Primack, J. R. 2000, ApJ, 528, 145
Guiderdoni, B., & Rocca-Volmerange, B. 1988, A&AS, 74, 185
Huang, J.-S., Cowie, L. L., Gardner, J. P., Hu, E. M., Songaila, A., & Wainscoat, R. J. 1997, ApJ, 476, 12
Huchra, J. 1999, in IAU Symp. 171, The Low Surface Brightness Universe, ed. J. I. Davies, C. Impey & S. Phillips (San Francisco: ASP), 45
Huchra, J. P., Geller, M. J., Clemens, C. M., Tokarz, S. P., & Michel, A. 1992, Bull. Inf. CDS, 41, 31
Jarrett, T.-H., Chester, T., Cutri, R., Schneider, S., Rosenberg, J., Huchra, J. P., & Mader, J. 2000a, AJ, 120, 298
Jarrett, T., Chester, T., Cutri, R., Schneider, S., Skrutskie, M., & Huchra, J. P. 2000b, AJ, 119, 2498
Johnson, H. L. 1966, ARA&A, 4, 193
Kauffmann, G., & Charlot, S. 1998, MNRAS, 297, L23
Kochanek, C. S., et al. 2000a, ApJ, 543, 131
Kochanek, C. S., Pahre, M. A., & Falco, E. E. 2000b, ApJ, submitted
Kron, R. G. 1980, ApJS, 43, 305
Kurtz, M. J., & Mink, D. J. 1998, PASP, 110, 934
Lilly, S. J., Tresse, L., Hammer, F., Crampton, D., & Le Fèvre, O. 1995, ApJ, 455, 108
Lin, H., Kirshner, R. P., Shectman, S. A., Landy, S. D., Oemler, A., Tucker, D. L., & Schechter, P. L. 1996, ApJ, 464, 60
Loveday, J. 2000, MNRAS, 312, 557
Loveday, J., Peterson, B. A., Efstathiou, G., & Maddox, S. J. 1992, ApJ, 390, 338
Maihara, T., et al. 2000, PASJ, 53, 25
Marinoni, C., Monaco, P., Giuricin, G., & Costantini, B. 1999, ApJ, 521, 50
Marzke, R. O., da Costa, L. N., Pellegrini, P. S., Willmer, C. N. A., & Geller, M. J. 1998, ApJ, 503, 617
Marzke, R. O., Geller, M. J., Huchra, J. P., & Corwin, H. G. 1994a, AJ, 108, 437
Marzke, R. O., Huchra, J. P., & Geller, M. J. 1994b, ApJ, 428, 43
McLeod, B. A., Bernstein, G. M., Rieke, M. J., Tollestrup, E. V., & Fazio, G. G. 1995, ApJS, 96, 117
Mobasher, B., Sharples, R. M., & Ellis, R. S. 1986, MNRAS, 223, 11
———. 1993, MNRAS, 263, 560
Moustakas, L. A., Davis, M., Grahan, J. R., Silk, J., Peterson, B. A., & Yoshii, Y. 1997, ApJ, 475, 445
Naim, A., et al. 1995a, MNRAS, 274, 1107
Naim, A., Lahav, O., Sodre, L., & Storrie-Lombardi, M. C. 1995b, MNRAS, 275, 567
Pahre, M. A., Djorgovski, S. G., & de Carvalho, R. R. 1999, ApJ, submitted
Ratcliffe, A., Shanks, T., Parker, Q. A., & Fong, R. 1998, MNRAS, 293, 197
Sandage, A., Tammann, G. A., & Yahil, A. 1979, ApJ, 232, 352
Saracco, P., Iovino, A., Garilli, B., Maccagni, D., & Chincarini, G. 1997, AJ, 114, 887
Schechter, P. 1976, ApJ, 203, 297
Schlegel, D. J., Finkbeiner, D. P., & Davis, M. 1998, ApJ, 500, 525
Shectman, S. A., Landy, S. D., Oemler, A., Tucker, D. L., Lin, H., Kirshner, R. P., & Schechter, P. L. 1996, ApJ, 470, 172
Skrutskie, M. F., et al. 1997, in The Impact of Large Scale Near-IR Sky Surveys, ed. F. Garzon et al. (Dordrecht: Kluwer), 187
Slonim, N., Somerville, R., Tishby, N., & Lahav, O. 2001, MNRAS, 323, 270
Soifer, B. T., et al. 1994, ApJ, 420, L1
Songaila, A., Cowie, L. L., Hu, E. M., & Gardner, J. P. 1994, ApJS, 94, 461
Sprayberry, D., Impey, C. D., Irwin, M. J., & Bothun, G. D. 1997, ApJ, 482, 104
Szokoly, G. P., Subbarao, M. U., Connolloy, A. J., & Mobasher, B. 1998, ApJ, 492, 452
Tonry, J. L., Blakeslee, J. P., Ajhar, E. A., & Dressler, A. 2000, ApJ, 530, 625
Vettolani, G., et al. 1997, A&A, 325, 954
Worthey, G. 1994, ApJS, 95, 107
York, D. G., et al. 2000 AJ, 120, 1579
Zucca, E., et al. 1997, A&A, 326, 477